THE JOURNAL OF PHYSICAL CHEMISTRY C

Article

pubs.acs.org/JPCC

Core and Valence Structures in $K\beta$ X-ray Emission Spectra of Chromium Materials

María Torres Deluigi,*[,†,‡] Frank M. F. de Groot,[§] Gastón López-Díaz,[†,⊥] Germán Tirao,[∥,⊥] Guillermo Stutz,[∥] and José Riveros de la Vega[∥,⊥]

[†]Departamento de Física, Universidad Nacional de San Luis, 5700 San Luis, Argentina

[‡]Facultad de Ciencias Exactas y Naturales, Universidad Nacional de Cuyo, 5500 Mendoza, Argentina

[§]Department of Chemistry, Utrecht University, Universiteitsweg 99, 3584CG Utrecht, The Netherlands

[∥]Facultad de Matemática, Astronomía y Física, Universidad Nacional de Córdoba, X5016LAE Córdoba, Argentina

[⊥]Consejo Nacional de Investigaciones Científicas y Técnicas, C1033AAJ Buenos Aires, Argentina

ABSTRACT: We analyze the core and valence transitions in chromium in a series of materials with a number of different ligands and including the oxidation states: Cr^{II}, Cr^{III}, Cr^{IV}, and Cr^{VI}. To study the core-to-core transitions we employ the CTM4XAS program and investigate the shapes, widths, intensities, and energy positions of the $K\beta_{1,3}$ and $K\beta'$ lines in each oxidation state. The theoretical spectra are compared with experimental data obtained with synchrotron radiation. We found that the $K\beta_{1,3}$ peak shifts to higher energy with increasing spin state. In addition, the widths of the $K\beta_{1,3}$ peak increases as the oxidation state decreases, which we explain from the increased spread of the multiplet structures. In the $K\beta'$ structure the presence of two peaks in Cr^{II}, Cr^{III}, and Cr^{IV} is due to the large 3p3d exchange interaction. For the analysis of the valence transitions we utilize the DV-$X\alpha$ method. We study the dependence of the relative intensities of the $K\beta''$ and $K\beta_{2,5}$ structures on symmetry, bond length, and the effective number of 3d and 4p electrons in different chemical environments.

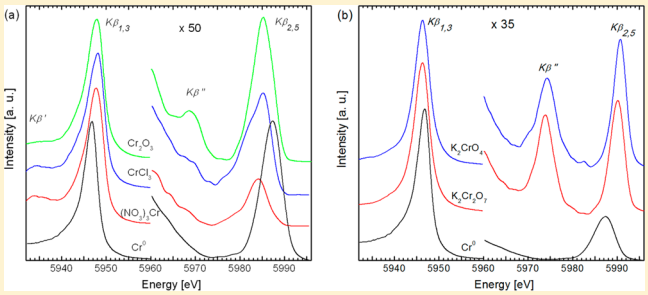

1. INTRODUCTION

Chromium is extensively used in the chemical industry in applications such as metal plating, leather tanning, pigments, or anticorrosion coatings. When assessing the potential toxicity of chromium, the concept of speciation must be emphasized: Cr^{III} is considered an essential micronutrient in the human diet. In contrast, Cr^{VI} is highly toxic and its compounds are considered human carcinogens. Therefore, the determination of chromium speciation in solid samples is critical for environmental and industrial purposes. Results have recently been published that evaluate the potential of the commercial wavelength-dispersive X-ray fluorescence spectrometer to perform practical quantitative speciation analysis of chromium in solid samples using Cr$K\beta$ X-ray emission spectroscopy (XES).[1]

In recent years, much progress has been achieved in the interpretation of the $K\beta$ X-ray emission spectrum of 3d transition metals.[2−11] It has been known for a long time that $K\beta$ emission spectra of 3d metals show a pronounced chemical sensitivity.[12−15] Two different regions can be distinguished in the $K\beta$ X-ray emission spectrum. The first region corresponds to the metal 3p core structure and consists of a $K\beta_{1,3}$ main line and a lower energy small peak $K\beta'$. The second structure corresponds to valence structure and contains two satellite lines: $K\beta_{2,5}$ directly below the Fermi level, and at lower energies $K\beta''$ or crossover peak. Figure 1 shows the experimental spectra including a detailed assignment.

The $K\beta'$ feature at lower energy is due to the (3p,3d) exchange interaction. It has also been assigned to either collective excitations or charge-transfer processes.[16,17] Photoemission spectroscopy on free atoms, however, shows that intra-atomic interactions dominate the $K\beta$ spectral shape.[18,19] Some authors consider that the $K\beta''$ satellite line originates as the result of a double vacancy process in the presence of a 3d spectator-hole.[20] Others believe it is the result of a plasmon excitation produced by a $K\beta_5$ photon.[21] However, it does not appear in metallic chromium. Alternatively, the $K\beta''$ peak has been assigned as ligand ns → metal 1s crossover transitions.[22] The present work confirms that the crossover peak should be considered as metal np → metal 1s transitions, where the metal np orbital character mixes with the ligand 2s states.

According to theoretical calculations, the $K\beta_5$ line is the s−d dipole forbidden transition when free atoms are considered,[23,24] since the $\Delta l = \pm 1$ condition is not satisfied. However, experimental data show a marked increase in the intensities of this line with the atomic number Z, and it is very strongly

Received: September 26, 2013
Revised: August 27, 2014
Published: August 29, 2014

   dx.doi.org/10.1021/jp409622r | J. Phys. Chem. C 2014, 118, 22202−22210

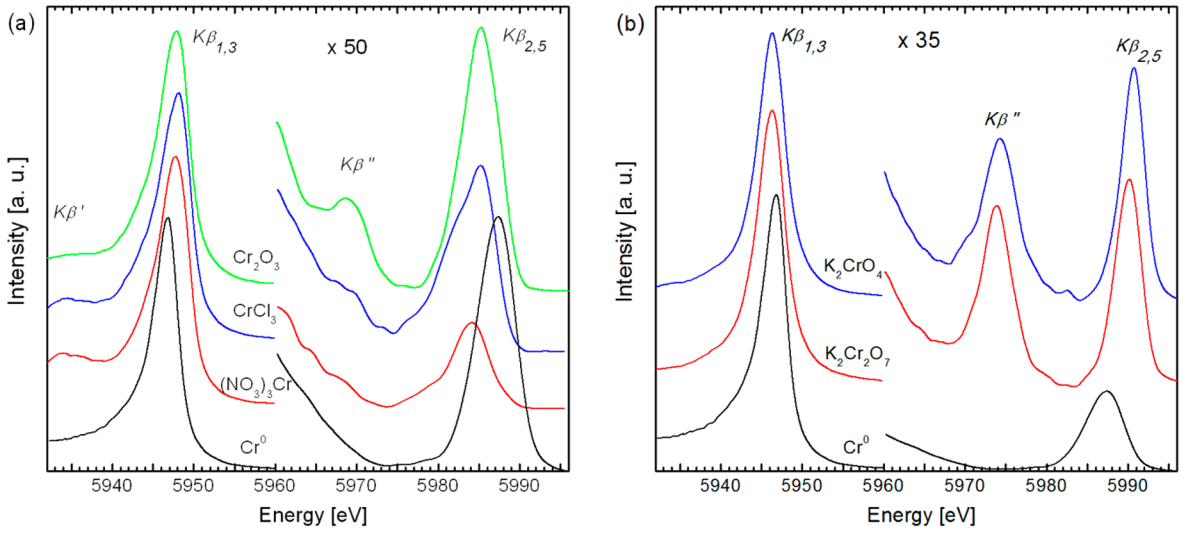

Figure 1. Experimental results of Cr $K\beta$ X-ray emission spectra. $K\beta_{1,3}$ relates to 1s3p X-ray emission, $K\beta''$ relates to the crossover peak (in oxides the oxygen 2s states) and $K\beta_{2,5}$ relates to valence band X-ray emission. Subpanel (a) includes Cr^0 and Cr^{III} compounds and (b) Cr^0 and Cr^{VI} compounds. The spectra are normalized to 1.0 at the maximum of the $K\beta_{1,3}$ peak.

enhanced around Z = 24 (chromium).[23] The origin of the $K\beta_5$ line is ascribed to transitions involving states that contain metal 3d character.[25−27] In the chromium compounds 4p states are partly occupied, implying that 4p → 1s transitions are possible (that correspond to $K\beta_2$ line). Recently, Eeckhout et al.[22] have demonstrated that Cr-3d states contribute very weakly to $K\beta_{2,5}$ structure in chromium compounds.

The valence XES technique is suitable for analyzing otherwise challenging samples such as amorphous, nanocrystalline and heterogeneous materials. Lancaster et al.,[28] by means of the study of iron $K\beta$ valence XES of nitrogenase, demonstrated that these data provide a signature for the presence and identity of the central atom in this catalyst. The presence of Cr−C bonds in the bulk structure of electrochemically deposited amorphous chromium coatings was confirmed by means of this technique.[22] Eeckhout et al.[22] also have shown that a contaminated soil sample most probably contains Cr carbides and/or phosphides from anthropogenic origin.

The main objective of this work is to study the core and valence structures of $K\beta$ emission spectra in chromium materials with different oxidation states: Cr^{II} ($3d^4$), Cr^{III} ($3d^3$), Cr^{IV} ($3d^2$), and Cr^{VI} ($3d^0$). In order to study the core-to-core transitions we employ the CTM4XAS program and investigated the shapes, widths, intensities, and energy positions of the $K\beta_{1,3}$ and $K\beta'$ peaks in each oxidation state. To analyze the valence structure we utilize the DV-$X\alpha$ method. In particular, we study the dependence of the relative intensities of $K\beta''$ and $K\beta_{2,5}$ satellite lines (with respect to the main $K\beta_{1,3}$ line) on symmetry, bond length, and effective number of 3d and 4p electrons in different chemical environments.

2. COMPUTATIONAL METHODS

The Cr $K\beta$ (1s 3p) core X-ray emission spectra were calculated with the charge transfer multiplet (CTM4XAS) program.[29] CTM4XAS assumes that the intermediate state can be described with the relaxed 1s core hole state, as has been used in most published $K\beta$ calculations.[30] It has been shown by Glatzel et al.[31] that the intermediate state should be described as the 1s photoemission state. For metallic and covalent systems the 1s photoemission spectra is dominated by the peak related to the lowest energy excited 1s core hole state.[32] In all, not-too-ionic systems where the 3d band is less than half-filled have the largest XPS intensity at their lowest energy excited 1s core state. An explicit calculation of the 1s photoemission spectrum of Cr_2O_3 shows that over 90% of the intensity is contained into a single peak related to the well-screened final state, which relates to a $1s^13d^5\underline{L}$ final state. The ground state has a $3d^3 + 3d^4\underline{L}$ configuration with $^4A_2$ symmetry. The excitation of a 1s electron will create a lowest energy state that consists of the configuration $1s^1\ 3d^3 + 1s^1\ 3d^4\underline{L}$, in which the symmetry of the $3d^3$ part of the state remains $^4A_2$. This state will obtain most of the intensity, and because for Cr_2O_3 the charge transfer energy Δ is approximately equal to the Hubbard U, the lowest energy state is close to 50% $1s^1\ 3d^3$ and 50% $1s^1\ 3d^4\underline{L}$. In the case of very ionic systems this reasoning does not always work because the poorly screened peak can have more intensity as the well screened peak.

In all Cr^{III}, Cr^{IV}, and Cr^{VI} materials, the weight of the well-screened peak will be higher than 90%. In the charge-transfer multiplet model, one starts with an atomic model.[33] The ground state of a 3d transition-metal ion can be described as a $3d^n$ configuration. When a 1s electron is excited to the continuum, the $K\beta$ emission spectrum can be calculated from the dipole transition matrix element for $1s^13d^n \rightarrow 3p^53d^n$ calculations. In the calculations, the energy levels of the initial state and final states are calculated and the spectrum is simulated by evaluating the dipole transition matrix elements. The initial state is influenced by the 3d−3d Coulomb interaction and the 1s−3d exchange interaction. In the final state, the multiplet splitting is determined from the 3d−3d Coulomb interaction, the spin−orbit coupling of the 3p hole and the 3p−3d Coulomb and exchange interaction. In the ligand-field multiplet model the effects of neighboring atoms are introduced via the crystal field in both the initial state and final state.

The valence X-ray emission spectrum is calculated from the transition of the 1s core state to the occupied metal p-character. The occupied metal p-character is determined with the DV-$X\alpha$ method. The crossover transitions are included in these calculations.[34]

dx.doi.org/10.1021/jp409622r | J. Phys. Chem. C 2014, 118, 22202−22210

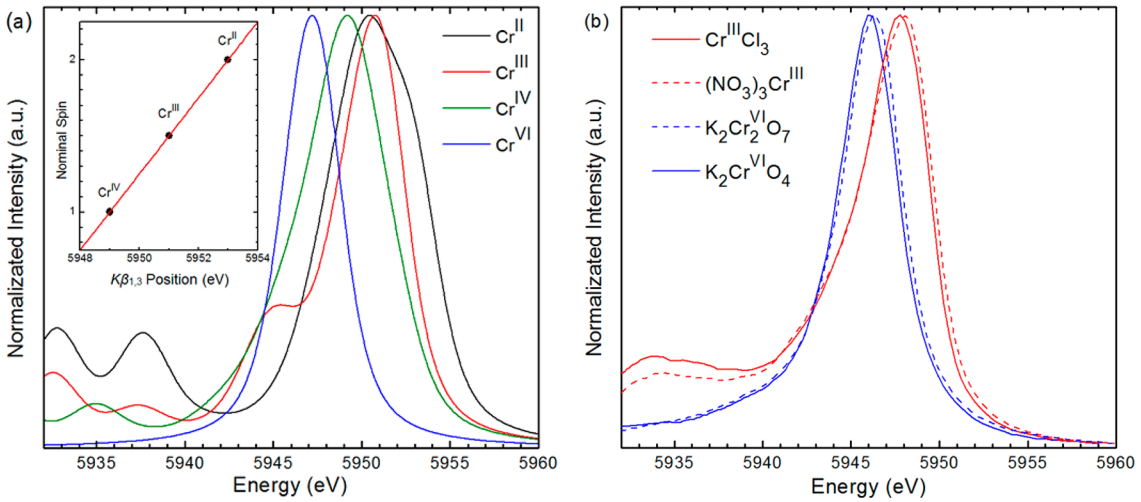

Figure 2. Comparison between theoretical and experimental results of the core Cr$K\beta$ spectra: (a) theoretical results from CTM4XAS program; (b) experimental results. The spectra are normalized to 1.0. The centers-of-gravity of all theoretical spectra are chosen to be identical and aligned to the experimental spectra.[3]

3. EXPERIMENTAL SECTION

$K\beta$ emission spectra of Cr^0 and some compounds of Cr^{III} and Cr^{VI} were measured using a Johann-type spectrometer[35] at the D12A-XRD1 beamline of the National Synchrotron Light Laboratory (LNLS), in Campinas, Brazil. The energy analysis of the fluorescence radiation was performed using a Si(333) analyzer with spherical focalization. The analyzer was scanned through the $K\beta$ spectrum, including both the $K\beta_{1,3}$ and the $K\beta_{2,5}$ emission lines of Cr. Analyzer, detector, and sample were arranged on a Rowland circle of 0.42 m diameter. The whole spectrometer was mounted in a vacuum chamber in order to avoid intensity losses due to absorption in the air and to reduce the background intensity from scattering in the air. 6.1 keV monochromatic radiation was used to excite the samples. Measurements were carried out using conventional 45°−45° reflection geometry. The instrumental energy resolution was evaluated in 1.6 eV ($K_2Cr_2O_7$ and K_2CrO_4) and 1.8 eV ($CrCl_3$, $(NO_3)_3Cr$ and Cr_2O_3) at the energy of the Cr$K\beta_{1,3}$ line. The spectrometer was calibrated using the $K\beta_{1,3}$ peak from a pure Cr sample. Its position was set to the energy value given by Bearden[36] (5946.71 eV). The sample holder was designed in such a way that the illuminated area on the sample is tangent to the Rowland circle at the same point for each sample. Stability and repeatability of the spectrometer was checked throughout the experiments by measuring the position of the $K\beta_{1,3}$ peak of Cr metal. Part of the experimental data was published elsewhere.[4,37,38]

4. RESULTS

Figure 1 shows an important dependence between the valence structure and oxidation state of chromium. In particular, the $K\beta''$ and $K\beta_{2,5}$ satellite lines have higher intensity in Cr^{VI} with respect to Cr^{III}. The $K\beta_{2,5}$ lines are broader in Cr^{III}, and their energies are around 5985 eV, whereas for Cr^{VI} are close to 5990 eV. The energy shift of the $K\beta_{2,5}$ line with respect to the same line in Cr^0 is more sensitive to the oxidation state that shift of the $K\beta_{1,3}$ line.[4]

A. Analysis of the $K\beta_{1,3}$ Line. Figure 2a,b shows theoretical and experimental results, respectively, of the core spectra. The theoretical calculations for Cr^{II}, Cr^{III}, Cr^{IV}, and Cr^{VI} have been performed with atomic values for the Slater integrals and the spin−orbit couplings, combined with a crystal field value of 0.6 times the formal valence. In these figures it is observed that the $K\beta_{1,3}$ peak position shifts to lower energies as the oxidation state increases. In experiment, the Cr^{III} peak is positioned at 5950 eV and the Cr^{VI} peak at 5946 eV. In the calculations the shift is from 5951 eV (Cr^{III} peak) to the Cr^{VI} peak at 5947 eV. It is noted that the $K\beta'$ structure has two peaks for Cr^{II}, Cr^{III}, and Cr^{IV} (Figure 2a).

In Figure 2a,b, it is observed that the $K\beta_{1,3}$ line of Cr^{III} has a weak shoulder on the low energy side. This shoulder arises from a spin flip in the metal valence shell.[31]

B. Analysis of the Valence XES Spectra. Table 1 shows the Cr compounds and the clusters used to perform the calculations with the DV-$X\alpha$ method. In each cluster, the central atom of Cr is surrounded by 4 or 6 ligand atoms organized in tetrahedral (T_d) and octahedral (O_h) symmetry, respectively. In the theoretical calculations, 1s−4p atomic orbitals have been used as basis functions for chromium, 1s−2p orbitals were used for oxygen, and 1s−3d were used for chlorine. Slater's exchange parameter was taken to be $\alpha = 0.7$ in all cases.

Table 1. Compounds Used for Calculations

compounds	oxidation state	symmetry	cluster	bond length a (Å)	ref
$CaCrO_4$	6	T_d	$[CrO_4]^{-2}$	1.60	39
K_2CrO_4	6	T_d	$[CrO_4]^{-2}$	1.65	39
$K_2Cr_2O_7$	6	T_d	$[CrO_4]^{-2}$	1.70	40
$CdCrO_4$	6	T_d	$[CrO_4]^{-2}$	1.78	41
CrO_3	6	T_d	$[CrO_4]^{-2}$	1.80	42
CrO_2	4	O_h	$[CrO_6]^{-8}$	1.90	43
$NaCrO_2$	3	O_h	$[CrO_6]^{-9}$	1.91	43
$CuCrO_2$	3	O_h	$[CrO_6]^{-9}$	1.99	44
Cr_2O_3	3	O_h	$[CrO_6]^{-9}$	2.00	41
CrO	2	O_h	$[CrO_6]^{-10}$	2.05	44
$Cs_3[Cr_2Cl_9]$	3	O_h	$[CrCl_6]^{-3}$	2.35	42
$Na_3[CrCl_6]$	3	O_h	$[CrCl_6]^{-3}$	2.36	40
$CrCl_3.6H_2O$	3	O_h	$[CrCl_6]^{-3}$	2.38	39
$Rb_2[CrCl_4]$	2	O_h	$[CrCl_6]^{-4}$	2.52	43
$CrCl_2$	2	O_h	$[CrCl_6]^{-4}$	2.55	45

dx.doi.org/10.1021/jp409622r | J. Phys. Chem. C 2014, 118, 22202−22210

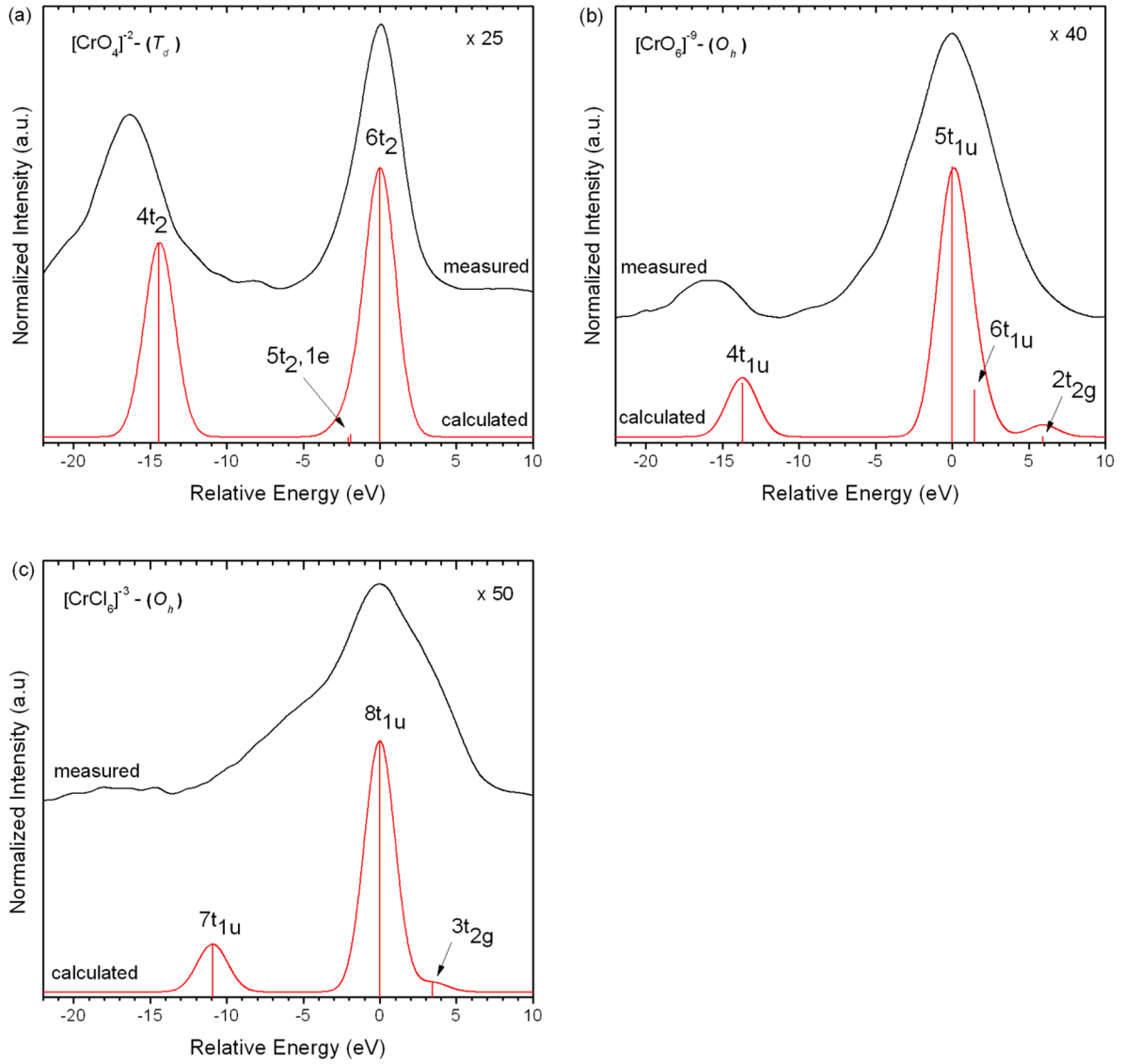

Figure 3. Comparison between theoretical and experimental Cr$K\beta$ spectra: (a) $[CrO_4]^{-2}$ with T_d symmetry corresponding to K_2CrO_4; (b) $[CrO_6]^{-9}$ with O_h symmetry corresponding to Cr_2O_3; (c) $[CrCl_6]^{-3}$ with O_h symmetry corresponding to $CrCl_3$. The theoretical spectra were shifted to align to the maximum of peak of the measured $K\beta_{2,5}$ emission. A Gaussian broadening of 1.0 eV was used.

Figure 3 shows the comparison between theoretical and experimental results of the Cr $K\beta$ spectrum; energies and intensities are relative to the main $K\beta_{1,3}$ line. The different components that contribute to $K\beta_{2,5}$ spectra are indicated in Figure 3.

In Figure 3, the lack of fitting concerning the peak splitting, and the broadening of the $5t_{1u}$ and $8t_{1u}$ peaks, should be assigned to the limitations of the DV-Xa code used. In particular, in our calculations we did not include the effects of electron spin. Besides, we only taken into account the coordination of one Cr atom including ligands up to the first coordination shell. Lee et al.[2] shown that changes in the spin state come to have pronounced contributions to both the intensity and energy distribution of the valence XES spectra of Fe.

It is possible to detail the leading coefficients or percentages of every atomic orbital in the formation of a specific MO. The results of such population analysis for the different clusters are shown in Table 2.Through the DV-Xα method, we corroborated that, for Cr compounds whose clusters have T_d symmetry, the $K\beta''$ and $K\beta_{2,5}$ lines are mainly generated through the transitions $4t_2 \rightarrow 1a_1$ and $6t_2 \rightarrow 1a$, respectively, which is in agreement with findings by other authors.[46,47]

For clusters with O_h symmetry, we found that radiative transitions of interest for this work originate in the MOs with t_{1u} symmetry. For all clusters with O_h symmetry, the $K\beta_{1,3}$ line originates in the $3t_{1u} \rightarrow 1a_{1g}$ transition, and the $K\beta''$ and $K\beta_{2,5}$ satellite lines mainly come from transitions $4t_{1u}/5t_{1u} \rightarrow 1a_{1g}$, respectively. The $2t_{2g}$ and $3t_{2g}$ MOs were found to be mainly composed of Cr-3d. These results are in agreement with the analysis of the density of Cr-3d states that were calculated for Cr_2O_3 by Eeckhout et al.[22] using FEFF8.2 calculations.

5. ANALYSIS AND DISCUSSION

A. Core XES Spectra. It is known that the core emission is sensitive to the metal spin state. More exactly, it reflects the effective number of unpaired metal 3d electrons. The shift of the $K\beta_{1,3}$ line is not caused by a change in nuclear screening between different oxidation states but by variations in the exchange splitting,[3] i.e., the $K\beta_{1,3}$ line position depends on the

dx.doi.org/10.1021/jp409622r | J. Phys. Chem. C 2014, 118, 22202−22210

Table 2. Mulliken Population Analysis of Cr Compounds

				AO (%)				
cluster	oxidation state	symmetry	MO	Cr-3p	Cr-3d	Cr-4p	O-2s	O-2p
$[CrO_4]^{-2}$		T_d	$3t_2$	98.72	...	0.04	0.60	0.65
			$4t_2$	0.73	3.08	1.77	93.72	0.70
	6		$5t_2$	0.09	37.73	0.02	3.01	59.15
			1e	...	40.41	...	...	59.58
			$6t_2$	0.30	0.65	5.44	0.66	92.95
$[CrO_6]^{-8}$		O_h	$3t_{1u}$	99.26	...	0.06	0.31	0.37
			$4t_{1u}$	0.27	...	1.04	96.84	1.84
	4		$5t_{1u}$	0.41	...	4.18	0.10	95.31
			$6t_{1u}$	0.16	...	0.51	1.23	98.10
			$2t_{2g}$	...	92.37	...	...	7.63
$[CrO_6]^{-9}$		O_h	$3t_{1u}$	99.46	...	0.05	0.21	0.28
			$4t_{1u}$	0.19	...	1.02	97.17	1.62
	3		$5t_{1u}$	0.56	...	4.50	0.51	94.43
			$6t_{1u}$	0.10	...	0.56	0.95	98.39
			$2t_{2g}$	...	92.14	...	...	7.86
$[CrO_6]^{-10}$		O_h	$3t_{1u}$	99.66	...	0.03	0.12	0.18
			$4t_{1u}$	0.11	...	0.91	97.64	1.35
	2		$5t_{1u}$	0.21	...	5.20	0.22	94.37
			$6t_{1u}$	0.05	...	0.46	0.65	98.84
			$2t_{2g}$	...	91.53	...	...	8.47
			MO	Cr-3p	Cr-3d	Cr-4p	Cl-3s	Cl-3p	Cl-3d
$[CrCl_6]^{-3}$	3	O_h	$6t_{1u}$	99.80	...	0.03	0.04	0.07	0.06
			$7t_{1u}$	0.05	...	1.68	98.20	0.03	0.04
			$8t_{1u}$	0.10	...	9.22	0.23	90.24	0.21
			$3t_{2g}$	...	85.15	...	...	13.20	1.64
$[CrCl_6]^{-4}$	2	O_h	$6t_{1u}$	99.91	...	0.02	0.01	0.03	0.03
			$7t_{1u}$	0.02	...	0.84	99.08	0.05	0.02
			$8t_{1u}$	0.04	...	6.02	...	93.88	0.06
			$3t_{2g}$	...	93.58	...	...	5.54	0.88

exchange interaction between the core hole and the unpaired spin in the valence shell as can be seen for the theoretical results found for the different oxidation states of Cr (see the inset in Figure 2a). Glatzel et al.[31] and Glatzel and Bergmann[3] found a similar behavior for Mn fluorides and oxides measured after photoionization.

In addition, the widths of the $K\beta_{1,3}$ line increases as the oxidation state decreases (see Figure 2a,b), because the multiplet structures are spread over a larger energy. In particular, as Cr^{II} is the d^4 high-spin state then this oxidation state has the widest $K\beta_{1,3}$ structure and largest shift to higher energy.

Table 3 shows the terms of the final states that contribute mainly to the intensity of the peaks which were obtained with the CTM4XAS program. For example, the lowest energy $1s^1$ $3d^4$ state of Cr^{II} has a ^4D configuration and its main $3d^4$ component is ^5D, i.e., equivalent to the ground state. Because the main contribution is the same every time as the ground state, these peaks behave similarly if a crystal field is applied, i.e., they are not sensitive to change of the ligand-field splitting (10Dq). The intensity of the peaks changes if the 3p3d multiplet effects are modified (cf. Figure 2a).

B. Valence XES Spectra. With the purpose of studying how the relative intensities of the $K\beta''$ and $K\beta_{2,5}$ satellite lines are related to effective number of 3d (N_{3d}) and 4p (N_{4p}) electrons and bond length (l), an elemental multivariate statistical analysis method was used. The degree of linear relationship for N pairs of data (x_1, y_1), ..., (x_N, y_N) can be measured through the following correlation coefficient:

Table 3. Principal Terms That Contribute to the Intensity of $K\beta'$[a]

	spin down spectra	
oxidation states	$1s^1$ $3d^n$	$3p^5$ $3d^n$
Cr^{II}	^4D (^5D)	^4F (^5D)
		^4P (^5D)
		^4D (^5D)
Cr^{III}	^3F (^4F)	^3F (^4F)
		^3D (^4F)
Cr^{IV}	^2F (^3F)	^2F (^3F)
		^2D (^3F)

[a]The first term symbol indicates the total symmetry of $3p^5$ $3d^n$ and the second term symbol gives the main contribution of the term symbols of the $3d^n$ configuration, according to the output of the Cowan program.[33]

$$r = \frac{N\sum_i x_i y_i - \sum_i x_i \sum_i y_i}{\sqrt{N\sum_i x_i^2 - (\sum_i x_i)^2}\sqrt{N\sum_i y_i^2 - (\sum_i y_i)^2}} \quad (1)$$

The r value is between 0 (when there is no correlation) and ±1 (when y_i can be expressed as a linear function of x_i). x_i (l, N_{3d} and N_{4p}) were considered to be parameters of the compound, and the y_i were considered to be the relative intensity of the $K\beta''$ and $K\beta_{2,5}$ lines. The values of N_{3d}, N_{4p}, l, and the theoretical relative intensities used in the calculations are shown in Table 4. The numbers of the effective electrons

dx.doi.org/10.1021/jp409622r | J. Phys. Chem. C 2014, 118, 22202−22210

Table 4. Relative Intensities of $K\beta''$ and $K\beta_{2,5}$ Peaks, Numbers of N_{3d} and N_{4p} Effective Electrons and l Bond Lengths

compound	oxidation state	symmetry	$IK\beta''/K\beta_{1,3}$	$IK\beta_{2,5}/K\beta_{1,3}$	N_{3d}	N_{4p}	l (Å)
$CaCrO_4$	6	T_d	3.88	4.94	3.52	0.39	1.60
K_2CrO_4	6	T_d	3.12	4.45	3.56	0.41	1.65
$K_2Cr_2O_7$	6	T_d	2.58	3.98	3.59	0.42	1.70
$CdCrO_4$	6	T_d	1.78	3.29	3.66	0.41	1.78
CrO_3	6	T_d	1.70	3.24	3.67	0.42	1.80
CrO_2	4	O_h	0.98	4.04	3.48	0.37	1.90
$NaCrO_2$	3	O_h	0.95	3.91	3.83	0.29	1.91
$CuCrO_2$	3	O_h	0.69	3.41	3.85	0.35	1.99
Cr_2O_3	3	O_h	0.66	3.40	3.85	0.36	2.00
CrO	2	O_h	0.52	2.97	4.41	0.28	2.05
$Cs_3[Cr_2Cl_9]$	3	O_h	0.65	3.50	4.20	0.65	2.35
$Na_3[CrCl_6]$	3	O_h	0.64	3.44	4.21	0.64	2.36
$CrCl_3.6H_2O$	3	O_h	0.61	3.35	4.21	0.63	2.38
$Rb_2[CrCl_4]$	2	O_h	0.34	2.38	4.57	0.42	2.52
$CrCl_2$	2	O_h	0.27	2.11	4.58	0.39	2.55

(N_{3d} and N_{4p}) were calculated by Mulliken's population analysis using the DV-Xα method.

The correlation coefficient between the relative intensity of $K\beta''$ peak ($IK\beta''/IK\beta_{1,3}$) and the bond length l for Cr−O compounds is $r = -0.83$. This correlation coefficient indicates that there is correlation between these parameters but that is not linear (see Figure 4), which agrees with the decreasing exponential trend found by Fazinić et al.[7]

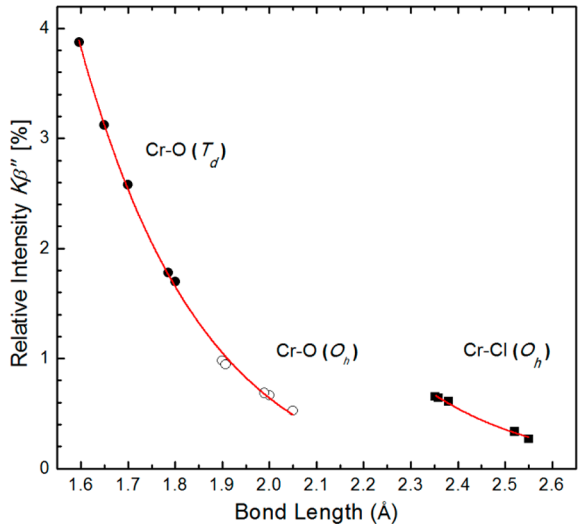

Figure 4. Relative intensities of the $K\beta''$ structure in relation to the $K\beta_{1,3}$ peak. Solid circles: Cr−O compounds with T_d symmetry; open circles: Cr−O compounds with O_h symmetry; solid squares: Cr−Cl compounds. The exponential fit (in red line) to the Cr−O data is $1800 \times e^{(-3.85l)} - 0.25$, $R^2 = 0.998$; and to the Cr−Cl data is $8500 \times e^{(-4.00l)} - 0.03$, $R^2 = 0.992$.

Then, the correlation between the relative intensities and l was analyzed in another way. Compounds were separated by ligand (O and Cl) and by symmetry (T_d or O_h). The results are shown in Table 5. The bond length l was found to be linearly correlated with the $IK\beta''/IK\beta_{1,3}$ and $IK\beta_{2,5}/IK\beta_{1,3}$ relative intensities of Cr−Cl compounds, with a negative slope; the bond length l was also found to be linearly correlated with $IK\beta_{2,5}/IK\beta_{1,3}$ of Cr−O compounds in the two symmetries, with a negative slope.

Table 5. Correlation Coefficients (r) between l and Relative Intensities of $K\beta''$ and $K\beta_{2,5}$ Peaks

ligand	symmetry	r (l vs $IK\beta''/IK\beta_{1,3}$)	r (l vs $IK\beta_{2,5}/IK\beta_{1,3}$)
O	T_d	−0.94	−0.99
	O_h	−0.94	−0.99
Cl	O_h	−1	−0.99

In Table 6 an almost linear relationship (i.e., r is very close to −1) could be observed to exist between $IK\beta''/IK\beta_{1,3}$ and N_{3d}

Table 6. Correlation Coefficient (r) between N_{3d} and $IK\beta''/IK\beta_{1,3}$, $IK\beta_{2,5}/IK\beta_{1,3}$, and between N_{4p} and $IK\beta_{2,5}/IK\beta_{1,3}$

ligand	symmetry	r (N_{3d} vs $IK\beta''/IK\beta_{1,3}$)	r (N_{3d} vs $IK\beta_{2,5}/IK\beta_{1,3}$)	r (N_{4p} vs $IK\beta_{2,5}/IK\beta_{1,3}$)
O	T_d	−0.91	−0.99	−0.77
	O_h	−0.84	−0.89	0.36
Cl	O_h	−0.98	−0.96	1

for Cr−Cl compounds, and also between $IK\beta_{2,5}/IK\beta_{1,3}$ and N_{3d} for Cr−O compounds with T_d symmetry. In the first case, where the N_{3d} influences on $IK\beta''/IK\beta_{1,3}$, this behavior can be explained by considering that the valence AOs of the Cl^- ion (Cl-3s and Cl-3p) have a larger radius than valence AOs O-2s and O-2p of the O^{2-} ($r_{Cl}{}^{-1} = 181$ pm and $r_O{}^{-2} = 140$ pm); consequently, the first result is more affected by the 3d valence electrons of the Cr atom. In the second case, N_{3d} plays a very important role in the $K\beta_{2,5}$ structure, since there is a covalent bond between Cr-3d and O-2p electrons in compounds with T_d symmetry.

A linear relationship with positive slope was found between $IK\beta_{2,5}/IK\beta_{1,3}$ and N_{4p} for Cr−Cl compounds. This behavior is due to the fact that a larger Cr-4p population participates in the $K\beta_{2,5}$ structure when a Cr−Cl bond occurs (with respect to a Cr−O bond), probably due to the size difference in the radius of the valence AOs on the two ligand atoms.

Therefore, if correlation coefficients for l, N_{3d}, and N_{4p} parameters are compared (Tables 5 and 6), the bond length would be the most appropriate parameter to analyze the relative intensities $IK\beta_{2,5}/IK\beta_{1,3}$ since it is near −1, irrespective of the ligand and the symmetry (see last column in Table 5). The numbers of N_{3d} and N_{4p} electrons are good correlation parameters, although it did not turn out to be that general.

dx.doi.org/10.1021/jp409622r | J. Phys. Chem. C 2014, 118, 22202−22210

Figure 4 shows that the intensities of the $K\beta''$ line are higher in the compounds with T_d symmetry than in those with O_h symmetry. This behavior is due to the existence of covalent Cr−O bonds producing a lower bond length, and thus greater interaction between the valence orbitals, resulting in increased transition probabilities for this transition.

This figure further shows that the relative intensities of the $K\beta''$ line vary continuously for Cr−O compounds when the symmetry is changed from T_d to O_h. This continuity is due to the participation of O-2s in the construction of $4t_2$ and $4t_{1u}$ MOs; the participation of O-2s in both MOs is approximately 94% and 97%, respectively (Table 2).

In return, in the case of $K\beta''$ structure for Cr−Cl compounds, the electron transition that generates the $K\beta''$ satellite line now originates from the $7t_{1u}$ MO, mainly formed by the Cl-3s. Therefore, the Cr−Cl compounds do not continue the same decreasing exponential trend, but rather show a different trend in Figure 4.

In Figure 5 theoretical relative intensities $IK\beta_{2,5}/IK\beta_{1,3}$ are shown in relation to the bond length. These results reveal three

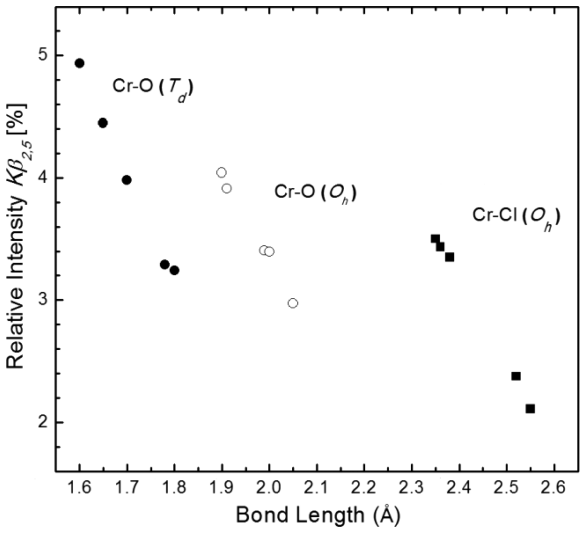

Figure 5. Relative intensities of the $K\beta_{2,5}$ structure in relation to the $K\beta_{1,3}$ peak. Solid circles symbols: Cr−O compounds with T_d symmetry; open circles symbols: Cr−O compounds with O_h symmetry; solid squares symbols: Cr−Cl compounds with O_h symmetry.

different trends: the first one corresponds to Cr−O compounds with T_d symmetry; the second one corresponds also to Cr−O compounds but with O_h symmetry, and the third one, to Cr−Cl compounds.

The $K\beta_{2,5}$ satellite line originates in 1e, $5t_2$, $6t_2 \rightarrow 1a_1$ transitions, and in particular for CrO_3 the contributions are 0.21% ($1e \rightarrow 1a_1$), 0.45% ($5t_2 \rightarrow 1a_1$) and 2.57% ($6t_2 \rightarrow 1a_1$). If we add them up, we obtain the relative intensity of the $K\beta_{2,5}$ line, which is 3.23% and is shown in Figure 5 for the bond length of CrO_3 (l = 1.80 Å). In Figure 5 this oxide has smaller relative intensity of the $K\beta_{2,5}$ line of Cr−O (T_d) compounds. The 1e and $5t_2$ MOs are formed by Cr-3d and O-2p, allowing quadrupole and dipole transitions which contribute to the $K\beta_{2,5}$ line. The small contributions of these MOs, which are observed in Figure 3a, are characteristics of clusters with T_d symmetry, and are due to a ∼60% contribution of O-2p in both MOs (Table 2). The contribution of the $6t_2$ MO, instead, is more intense than the previous due to the fact that there is a major contribution from O-2p (92.95%) in this MO; there is also a minor participation of Cr-4p (see Table 2).

The $[CrO_6]^{-8}$ cluster of the CrO_2 oxide presents O_h symmetry, and mainly the relative intensity of the $K\beta_{2,5}$ satellite line originates in the $5t_{1u}$, $6t_{1u} \rightarrow 1a_{1g}$ transitions. Since the cluster has O_h symmetry, there is also a small contribution to the relative intensity from the $2t_{2g}$ MO. The values of contributions are 3.01% ($5t_{1u} \rightarrow 1a_{1g}$), 0.85% ($6t_{1u} \rightarrow 1a_{1g}$), and 0.13% ($2t_{2g} \rightarrow 1a_{1g}$), respectively. The sum of those values results in the relative intensity of the $K\beta_{2,5}$ line, which is 4.04% and is shown in Figure 5 for the bond length of CrO_2 (l = 1.90 Å). In Figure 5 this oxide has higher relative intensity of the $K\beta_{2,5}$ line of Cr−O (O_h) compounds. The largest contribution to the relative intensity from the $5t_{1u}$ MO is characteristic of this type of symmetry in the Cr−O compounds, and it is due to the major participation (95.31%) of the O-2p AO. In addition, Cr-4p has a greater participation in the formation of this MO, as compared to the case of the T_d cluster in the previous paragraph ($5t_2$ MO), generating a greater dipole transition probability (see Table 2). The less contribution of the $6t_{1u}$ MO to the $K\beta_{2,5}$ intensity, in relation to the $5t_{1u}$ MO, is due to a smaller participation of the Cr-4p.

In the $2t_{2g}$ MO the O-2p participation is lowest with respect to $5t_{1u}$ and $6t_{1u}$ MOs, generating a lower dipolar transition probability. In addition, there is a quadrupole contribution to the intensity of the $K\beta_{2,5}$ line, due to greater participation of the Cr-3d (Table 2) and relatively little mixing between the Cr-3d and O-2p AOs, which is according with the calculations performed to Eeckhout et al.[22] using the FEFF8.2 code.

Then, we found that the intensities of the $K\beta_{2,5}$ line, which originate mainly in transitions from the $6t_2$ and $5t_{1u}$ MOs, are mostly formed by O-2p in the two symmetries, T_d and O_h, respectively. In addition, the results of the Mulliken population analysis show that the major contribution of O-2p in clusters with T_d symmetry corresponds to the p_x and p_z components. While for clusters with O_h symmetry, the only contribution is from the p_x component; in this way, $K\beta_{2,5}$ oscillator strength comes mainly from O-$2p_x$. Therefore, the discontinuity observed in Figure 5 for Cr−O compounds, is due to $5t_{1u}$ MO is formed entirely by O-$2p_x$.

The third trend for the higher l values in Figure 5 corresponds to the Cr−Cl compounds. This trend appears because the transition that generates the $K\beta_{2,5}$ line now originates from the Cl-3p, which mostly participates in the formation of the $8t_{1u}$ MO.

As shown in Figure 5, the relative intensities of the $K\beta_{2,5}$ lines in the Cr−Cl compounds, for the smallest l values, are similar to those of the Cr−O compounds, even when the bond length is higher than in the first ones. This is due to two reasons: in the first place, because of the larger size of Cl-3p as compared to O-2p; and in the second place, because of the larger contribution of the Cr-4p in the $8t_{1u}$ MO in relation to the $5t_{1u}$ of the Cr−O compounds (see Table 2).

6. CONCLUSIONS

Core and valence structures of the Cr $K\beta$ X-ray emission spectra were studied theoretically and compared with experimental spectra. The calculations of core structure ($K\beta'$ and $K\beta_{1,3}$ peaks) were performed with the CTM4XAS 5.5 program, and for valence structure ($K\beta''$ and $K\beta_{2,5}$ peaks) with the DV-Xα method. The main results are summarized below:

We found for Cr compounds that the $K\beta_{1,3}$ peak shifts to higher energy when spin state increased (i.e., when oxidation

states decrease). Besides, the theoretical and experimental widths of the $K\beta_{1,3}$ increases as the oxidation state decreases because the multiplet structures are spread over a larger energy.

In the $K\beta'$ structure the presence of two peaks in Cr^{II}, Cr^{III}, and Cr^{IV} is due to large 3p3d multiplet effects (including the exchange) which create multiple states with the same symmetry as the ground state (see Table 3). Besides, we found that the intensity of $K\beta'$ structure increases as the oxidation state decreases, because the 3p3d multiplet effects increase.

The differences in both experimental and theoretical energies among the $K\beta_{2,5}$ and $K\beta''$ lines for the Cr−O compounds are 16 and 14 eV, respectively. These values are very near the differences between the ionization energies of the 2s and 2p orbitals of O (15 eV). This confirms that said lines meanly originate in the AOs of the Cr ligands.

Bond length was found to be the appropriate parameter to analyze the $IK\beta_{2,5}/IK\beta_{1,3}$ relative intensities, since the linear correlation parameter is near −1 for each symmetry and each ligand (see Tables 5, 6, and Figure 5). It is also the case for studying $IK\beta''/IK\beta_{1,3}$ when the ligand is Cl, since in this case, $r = -1$ (see Figure 4). The N_{3d} and N_{4p} are also good correlation parameters, but they are not that general.

We found that the relative intensities of the $K\beta''$ line in the clusters with T_d symmetry are always higher than those with O_h symmetry because of the shorter Cr−O distance (see Figure 4). The existence of a covalent bond in the Cr−O compounds with T_d symmetry generates a strong interaction between the Cr valence orbitals and the O-2s AO. This increases the probabilities of the $4t_2 \rightarrow 1a_1$ transition, as revealed from the relative intensities of the $K\beta''$ satellite line.

The $K\beta''$ dipolar oscillator strengths came from mainly O-2s and Cl-3s for compounds studied. A smaller contribution came from Cr-3p and Cr-4p.

The $K\beta_{2,5}$ line is mainly originated in transitions from the $6t_2$ and $5t_{1u}$ MOs, which mostly formed by O-2p. The discontinuity observed when changing the symmetry in the Cr−O compounds (Figure 5) is due to $5t_{1u}$ MO is formed entirely by O-2p_x, in agreement with the Mulliken population analysis. In contrast to the behavior that we found for the $K\beta''$ line (Figure 4) in the Cr−O compounds (which present a continuous trend when the symmetry of the cluster changes), this is due to the fact that the $4t_2$ and $4t_{1u}$ MOs are mostly formed by O-2s (see Table 2).

In the $K\beta_{2,5}$ structure, the OMs with $2t_{2g}$ and $3t_{2g}$ symmetries were found to be mostly composed by population of Cr-3d, which would produce a quadrupole contribution to this structure.

AUTHOR INFORMATION

Corresponding Author

*E-mail: charo@unsl.edu.ar.

Notes

The authors declare no competing financial interest.

ACKNOWLEDGMENTS

This work has been supported by the Brazilian Synchrotron Light Laboratory (LNLS). Dr. Torres Deluigi wish to especially thank Dr. Kazuo Taniguchi for having allowed her to access the DV-$X\alpha$ method, and Dr. Takeshi Mukoyama for having taught her to use the DV-$X\alpha$ method, and for his helpful and permanent and advice.

REFERENCES

(1) Malherbe, J.; Claverie, F. *Anal. Chim. Acta* **2013**, *773*, 37−44.
(2) Lee, N.; Petrenko, T.; Bergmann, U.; Neese, F.; DeBeer, S. *J. Am. Chem. Soc.* **2010**, *132*, 9717−9727.
(3) Glatzel, P.; Bergmann, U. *Coord. Chem. Rev.* **2005**, *249*, 31−63.
(4) Torres Deluigi, M.; Tirao, G.; Stutz, G.; Cusatis, C.; Riveros, A. *J. Chem. Phys.* **2006**, *325*, 477−484.
(5) Fazinić, S.; Jakšić, M.; Mandić, L.; Dobrinić, J. *Phys. Rev. A* **2006**, *74*, 062501.
(6) Mandić, L.; Fazinić, S.; Jakšić, M. *Phys. Rev. A* **2009**, *80*, 042519.
(7) Fazinić, S.; Mandić, L.; Kavčič, M.; Božičević, I. *Spectrochim. Acta, Part B* **2011**, *25*, 461−469.
(8) Hölzer, G.; Fritsch, M.; Deutsch, M.; Härtwig, J.; Förster, E. *Phys. Rev. A* **1997**, *56*, 4554.
(9) Mukoyama, T.; Taniguchi, K.; Adachi, H. *Phys. Rev. A* **2001**, *63*, 042514.
(10) Kavčič, M.; Budnar, M.; Mühleisen, A.; Török, I. *Nucl. Instrum. Methods B* **1998**, *136−138*, 173−178.
(11) Uršič, M.; Kavčič, M.; Budnar, M. *Nucl. Instrum. Methods B* **2003**, *211*, 7−14.
(12) Bergmann, U.; Bendix, J.; Glatzel, P.; Gray, H. B.; Cramer, S. P. *J. Chem. Phys.* **2002**, *116*, 2011−2015.
(13) Gallo, E.; Lamberti, C.; Glatzel, P. *Phys. Chem. Chem. Phys.* **2011**, *13*, 19409−19419.
(14) Safonov, V. A.; Vykhodtseva, L. N.; Polukarov, Y. M.; Safonova, O. V.; Smolentsev, G.; Sikora, M.; Eeckhout, S. G.; Glatzel, P. *J. Phys. Chem. B* **2006**, *110*, 23192.
(15) Tsutsumi, K.; Nakamori, H.; Ichikawa, K. *Phys. Rev. B* **1976**, *13*, 929−933.
(16) Deutsch, M.; Hölzer, G.; Härtwig, J.; Wolf, J.; Fritsch, M.; Förster, E. *Phys. Rev. A* **1995**, *51*, 283−296.
(17) Kawai, J.; Takami, M.; Satoko, C. *Phys. Rev. Lett.* **1990**, *65*, 2193−2196.
(18) Sonntag, B.; Zimmermann, P. *Rep. Prog. Phys.* **1992**, *55*, 911−987.
(19) Ankudinov, A. L.; Nesvizhskii, A. I.; Rehr, J. J. *J. Synchrotron Radiat.* **2001**, *8*, 92−95.
(20) Enkisch, H.; Sternemann, C.; Paulus, M.; Volmer, M.; Schülke, W. *Phys. Rev. A* **2004**, *70*, 022508.
(21) Gokhale, B. G.; Rai, S.; Rai, S. D. *J. Phys. F* **1977**, *7*, 299−301.
(22) Eeckhout, S. G.; Safonova, O. V.; Smolentsev, G.; Biasioli, M.; Safonov, V. A.; Vykhodtseva, L. N.; Sikora, M.; Glatzel, P. *J. Anal. At. Spectrom.* **2009**, *24*, 215−223.
(23) Török, I.; Papp, T.; Pálinkás, J.; Budnar, M.; Mühleisen, A.; Kawai, J.; Campbell, J. L. *Nucl. Instrum. Methods B* **1996**, *114*, 9−14.
(24) Scofield, J. H. *At. Data Nucl. Data Tables* **1974**, *14*, 121−137.
(25) Agarwal, B. K. *X-Ray Spectroscopy: An Introduction*, 2nd ed.; Springer Series in Optical Sciences; Springer: Berlin, 1991; p 100.
(26) Okura, T.; Kanazawa, T. *J. Mater. Sci. Lett.* **1990**, *9*, 790−792.
(27) Kawai, J. *J. Mater. Sci. Lett.* **1992**, *11*, 1096−1098.
(28) Lancaster, K. M.; Roemelt, M.; Ettenhuber, P.; Hu, Y.; Ribbe, M. W.; Neese, F.; Bergmann, U.; DeBeer, S. *Science* **2011**, *334*, 974−977.
(29) Stavitski, E.; de Groot, F. M. F. *Micron* **2010**, *41*, 687−918.
(30) Peng, G.; de Groot, F. M. F.; Hämäläinen, K.; Moore, J. A.; Wang, X.; Grush, M. M.; Hastings, J. B.; Siddons, D. P.; Armstrong, W. H.; Mullins, O. C.; Cramer, S. P. *J. Am. Chem. Soc.* **1994**, *116*, 2914−2920.
(31) Glatzel, P.; Bergmann, U.; de Groot, F. M. F.; Cramer, S. P. *Phys. Rev. B* **2001**, *64*, 045109.
(32) Juhin, A.; de Groot, F.; Vankó, G.; Calandra, M.; Brouder, C. *Phys. Rev. B* **2010**, *81*, 115115.
(33) Cowan, R. D. *The Theory of Atomic Structure and Spectra*; University of California Press: Berkeley, 1981.
(34) Mukoyama, T.; Taniguchi, K.; Adachi, H. *Phys. Rev. B* **1986**, *34*, 3710−3716.
(35) Tirao, G.; Stutz, G.; Cusatis, C. *J. Synchrotron Rad.* **2004**, *11*, 335−342.
(36) Bearden, J. A. *Rev. Mod. Phys.* **1967**, *39*, 78−124.

(37) Tirao, G.; Torres Deluigi, M.; Ceppi, S.; Stutz, G.;Riveros, J. A. *Avances en Análisis por Técnicas de Rayos X*, Vol. *XIV*, 2008; pp 313−319 (Proceedings of the 10th Latin American Seminar on Analysis by X-Ray Techniques, Arica, Chile). In Spanish.
(38) Tirao, G.; Torres Deluigi, M.; Stutz, G.; Cusatis, C.; Riveros, J. *Brazilian Synchrotron Light Laboratory (LNLS) Activity Report 2004*, 2005
(39) Collotti, G.; Conti, L.; Socchi, M. *Acta Crystallogr.* **1959**, *12*, 416.
(40) Wyckoff, R. W. G. *Crystal Structures*; Interscience: New York, 1953.
(41) Newnham, R. E.; Dehaan, Y. M. *Z. Kristallogr., Kristallgeom., Kristallphys., Kristallchem.* **1962**, *117*, 235−237.
(42) Bystrom, A.; Wilhelmi, K. *Acta Chem. Scand.* **1950**, *4*, 1131−1141.
(43) Bauer, W. H. *Acta Crystallogr., Sect. B* **1976**, *32*, 2200−2204.
(44) Oswald, H. R. *Helv. Chim. Acta* **1961**, *44*, 1049−1054.
(45) Wooster, N. *Z. Kristallogr., Kristallgeom., Kristallphys., Kristallchem.* **1930**, *74*, 363−374.
(46) Adachi, H.; Tsukada, K.; Satoko, C. *J. Phys. Soc. Jpn.* **1978**, *45*, 875−883.
(47) Mukoyama, T.; Taniguchi, K.; Adachi, H. *Bull. Inst. Chem. Res., Kyoto Univ.* **1984**, *62*, 13−16.